J Appl Electrochem (2009) 39:1565–1572
DOI 10.1007/s10800-009-9842-1

ORIGINAL PAPER

Effect of AB_5 alloy on $Ti_{0.10}Zr_{0.15}V_{0.35}Cr_{0.10}Ni_{0.30}$ hydrogen storage alloy

Yanzhi Wang · Minshou Zhao · Limin Wang

Received: 30 April 2008 / Accepted: 16 February 2009 / Published online: 28 February 2009

Abstract The structure and electrochemical characteristics of melted composite $Ti_{0.10}Zr_{0.15}V_{0.35}Cr_{0.10}Ni_{0.30} + x\%$ $LaNi_4Al_{0.4}Mn_{0.3}Co_{0.3}$ ($x = 0, 1, 5$) hydrogen storage alloys have been investigated systematically. XRD shows that though the main phase of the matrix alloy remains unchanged after $LaNi_4Al_{0.4}Mn_{0.3}Co_{0.3}$ alloy is added, a new specimen is formed. The amount of the new specimen increases with increasing x. SEM-EDS analysis indicates that the V-based solid solution phase is mainly composed of V, Cr and Ni; C14 Laves phase is mainly composed of Ni, Zr and V; the new specimen containing La is mainly composed of Zr, V and Ni. The electrochemical measurements suggest that the activation performance, the low temperature discharge ability, the high rate discharge ability and the cyclic stability of composite alloy electrodes increase greatly with the growth of x. The HRD is controlled by the charge-transfer reaction of hydrogen and the hydrogen diffusion in the bulk of the alloy under the present experimental conditions.

Keywords Composite alloy · Hydrogen storage alloys · V-based solid solution alloy · Metal hydride electrode · Electrochemical characteristics

List of symbols

XRD	X-ray diffraction
SEM	Scanning electron microscopy
EDS	Energy-dispersive spectrometer
C_{max}	Maximum discharge capacity (mAh g^{-1})
C_n	Discharge capacity at cycle number n (mAh g^{-1})
S_n	Capacity retention at cycle number n
C_T	Discharge capacity at certain temperature (mAh g^{-1})
C_{303}	Discharge capacity at 303 K (mAh g^{-1})
LTD	Low temperature discharge ability
HTD	High temperature discharge ability
HRD	High-rate dischargeability
C_i	Discharge capacity at different discharge rate (mAh g^{-1})
C_{60}	Discharge capacity at both the charge/discharge current density of 60 mA g^{-1} (mAh g^{-1})
DOD	Depth of discharge (%)
EIS	Electrochemical impedance spectroscopy
R_{ct}	Charge-transfer resistance (mΩ)
I_0	Exchange current density (mA g^{-1})
R	Gas constant (J mol^{-1} K^{-1})
T	Absolute temperature (K)
F	Faraday constant (C mol^{-1})
D	Hydrogen diffusion coefficient (cm^2 s^{-1})

1 Introduction

Up to now, certain hydrogen storage electrode alloys have been extensively researched and developed, including the rare earth-based AB_5 and AB_3 type alloys, Ti- and Zr-based AB_2 type alloy, Mg-based alloy and V-based solid solution alloy. Among these types of alloys, V-based solid solution alloys are expected as a highly promising hydrogen storage

Y. Wang · M. Zhao
College of Environmental and Chemical Engineering, Yanshan University, 066004 Qinhuangdao, China

M. Zhao (✉) · L. Wang
State Key Laboratory of Rare Earth Resources Utilization, Changchun Institute of Applied Chemistry, CAS, 5625 Renmin Street, 130022 Changchun, China
e-mail: hhwyz@ysu.edu.cn

materials due to their relatively high hydrogen storage capacity and the capability of absorbing and desorbing hydrogen reversibly under ambient conditions [1–5]. The hydrogenation and dehydrogenation property of the hydrogen storage alloys in alkaline electrolyte is very important for its electrochemical properties, including the activation property, electrochemical capacity, the high-rate discharge ability and cycling characteristics, etc. However, except for Ti–V-Ni-based solid solution alloy, they cannot be used as electrode alloys as a result of poor electro-catalytic activity and high rate of dissolution of vanadium [6, 7]. In recent years, many researchers have been interested in Ti–Cr-V-based solid solution alloys because maximum hydrogen storage capacity of the alloy reaches about 3.7 wt.%, but the rechargeable hydrogen storage capacity is limited to only about half of that. It is reported that the hydriding property of the alloy has been improved by surface modification [8], annealing treatment [9] and additive elements [10–13].

Recently, it is reported that additive AB_5 alloy with easy initial activation, long cycle life, better electrochemical hydrogen storage capacity is helpful to improve both the hydrogen reaction kinetics and the discharge capacity of AB_2 alloy through composition optimum [14–18]. In this paper, effect of $LaNi_4Al_{0.4}Mn_{0.3}Co_{0.3}$ alloy addition on the structure and electrochemical characteristics of $Ti_{0.10}Zr_{0.15}V_{0.35}Cr_{0.10}Ni_{0.30}$ solid solution alloy is investigated systematically.

2 Experimental details

$Ti_{0.10}Zr_{0.15}V_{0.35}Cr_{0.10}Ni_{0.30}$ alloy (referred to as TVS hereafter) and $LaNi_4Al_{0.4}Mn_{0.3}Co_{0.3}$ alloy (referred to as AB_5 hereafter) were prepared by arc melting of the constituent elements on a water-cooled copper hearth under argon atmosphere, respectively. The purity of the starting elemental metal was higher than 99.5%. The ingots were turned over and re-melted three times for homogeneity. Then the compressed mixtures of TVS alloy and AB_5 alloy in the mass ratio of 9.9:0.1, 9.5:0.5 were arc-melted respectively under 0.06 MPa Ar atmosphere four times to ensure composition homogeneity. The melted composite TVS + x% AB_5 (x = 0, 1, 5) alloys were mechanically crushed in air and ground into powder in an agate mortar. The composite alloy powders of 300 mesh size were used for electrochemical measurements; the composite alloy powders of 400 mesh were used for XRD analysis with Cu $K\alpha$ radiation on D/Max-rB X-ray diffractometer with the help of Jade 5 software. The morphologies of the alloys were observed under KYKY2800-type scanning electron microscopy (SEM). The composition of the phases for the composite alloy was analyzed by a Kevex-sigma Level 4 energy-dispersive spectrometer (EDS).

The tested electrodes were fabricated by mixing the composite alloy powder (150 mg) with carbonyl nickel powder (750 mg). The mixture was then pressed into a pellet (10 mm in diameter and about 1.5 mm in thickness) under a pressure of 15 MPa. Electrochemical measurements were performed in a standard open tri-electrode electrolysis cell which consisted of a working electrode (the MH pellet electrode), a sintered $Ni(OH)_2$/NiOOH counter electrode with excess capacity, and a Hg/HgO reference electrode immersed in 6 mol/L KOH electrolyte. The charge/discharge tests were carried out with DC-5 battery testing instrument under computer control. The low temperature discharge ability was measured after being fully charged at constant temperature using low-temperature-equipment (WGD701). During the charge/discharge, the electrodes were fully charged (the over-charged ratio approximately 30%) at a current density of 60 mA g^{-1}, and then discharged at 60 mA g^{-1} to the cut-off potential of −0.6 V versus Hg/HgO.

After the test electrodes were completely activated, the electrochemical impedance spectroscopy (EIS) measurements were conducted at 50% depth of discharge (DOD) at 303 K with a Solartron 1287 Potentiostat/Galvanostat and a Solartron 1255 frequency response analyzer through Z-POLT software. The EIS spectra were obtained in the frequency range 0.1 Hz to 1 MHz with an ac amplitude perturbation of 5 mV under open circuit conditions.

After being fully charged and 30 min open-circuit lay-aside, the hydrogen diffusion coefficient was determined by the potential step method, which was performed at a constant potential of +500 mV for 2,500 s on the E.G&G PARC Model 273 Potentiostat/Galvanostat.

3 Results and discussion

3.1 Crystallographic structure and microstructure

Figure 1 shows XRD patterns of the as-cast AB_5 and TVS + x% AB_5 (x = 0, 1, 5) alloy. The matrix phase structure of TVS alloy composing of V-based solid solution phase with a BCC structure and C14 Laves phase with $MgZn_2$-type hexagonal structure is unchanged after AB_5 alloy is added. However, the diffraction data reveals that the individual peaks are slightly different. Also the new specimen is indicated by a small additional peak which increases gradually with increasing AB_5 alloy addition, which is confirmed by the SEM (see Fig. 2) and EDS analysis (see Fig. 3 and Table 2). The lattice parameters and cell volumes of the main phase for each alloy were calculated and are listed in Table 1. The lattice parameters and cell volumes of the BCC phase and C14 Laves phase increase as x increases from 0 to 1 and decrease as x

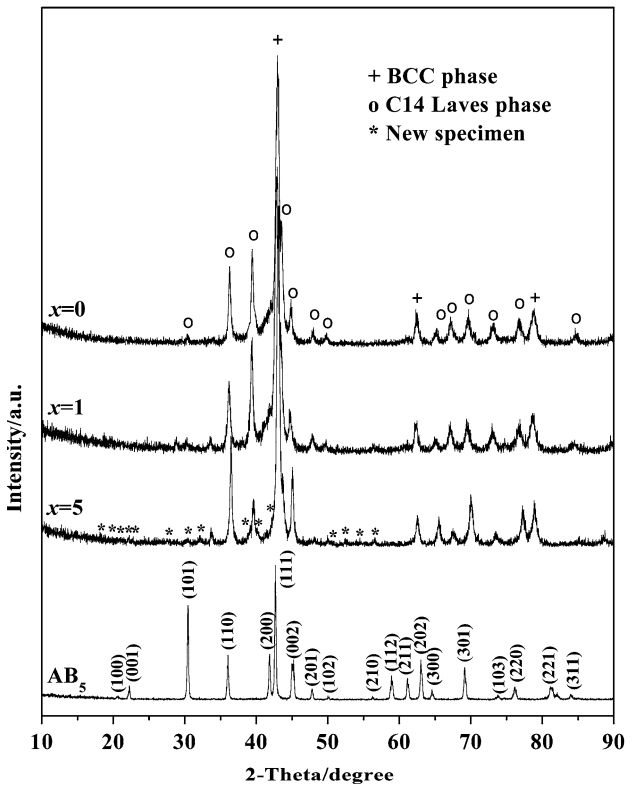

Fig. 1 XRD pattern of AB_5 and TVS + x% AB_5 (x = 0, 1, 5) alloy

increases further. Formation of the new specimen and changes of the lattice parameters of the main phase would impact on the electrochemical properties of each alloy.

Figure 2 presents SEM micrograph of the composite TVS + x% AB_5 (x = 1, 5) alloy. Figure 3 shows EDS pattern of TVS + 5% AB_5 alloy. Table 2 summarizes EDS results obtained from the main phase and the new specimen (white lard phase) which is on the TVS + 5% AB_5 alloy surface. It is clear that the composite alloy contains three

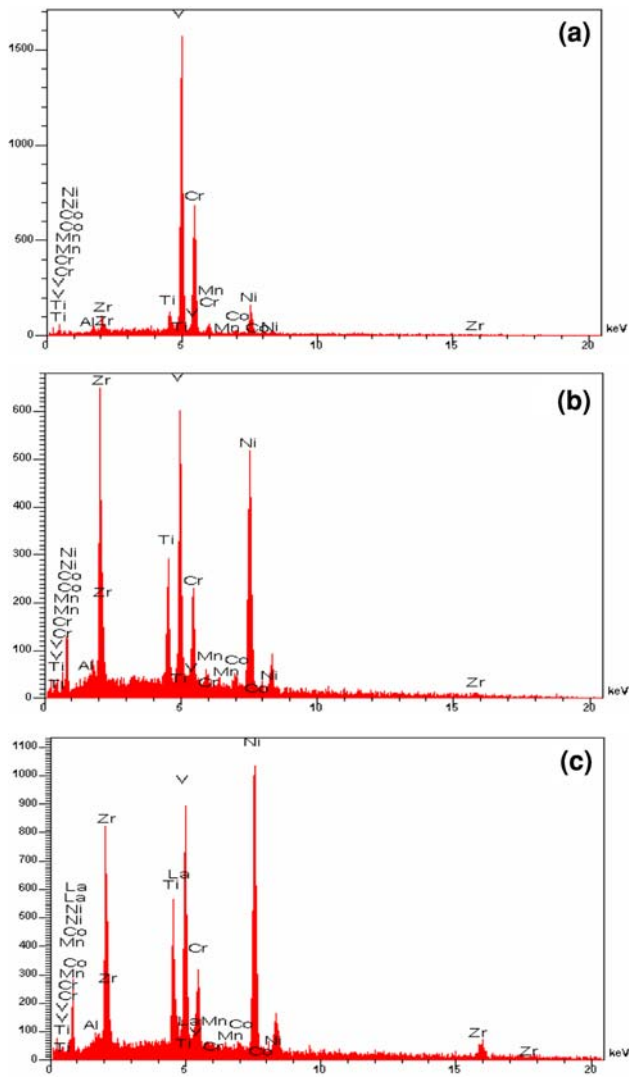

Fig. 3 EDS analysis of TVS + 5% AB_5 alloy: **a** BCC phase; **b** C14 Laves phase; **c** new specimen

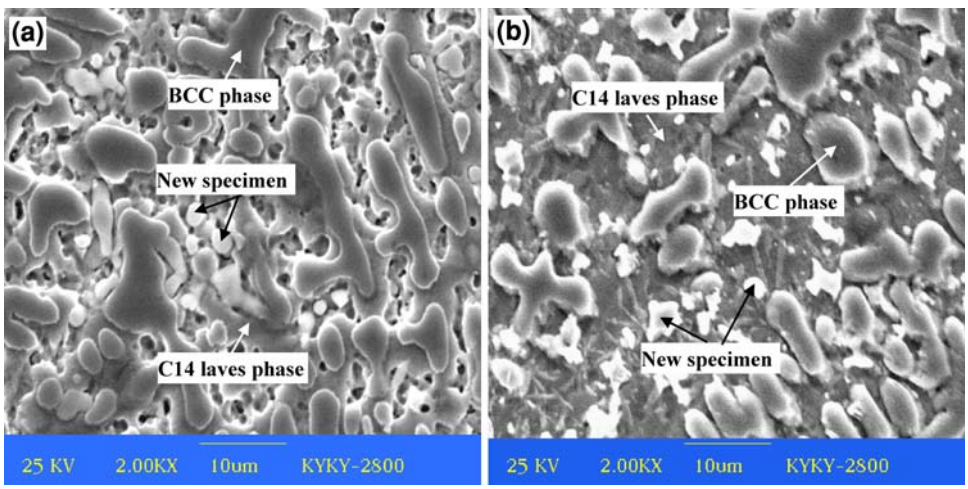

Fig. 2 SEM micrograph and EDS analysis of TVS + x% AB_5 (x = 1, 5) alloy: **a** x = 1; **b** x = 5

Table 1 Lattice parameters of BCC phase and C14 Laves phase in the composite

x	Phase	Lattice parameter		Cell volume (nm^3)
		a (nm)	c (nm)	
0	BCC	0.2969	0.8093	0.02617
	C14 Laves	0.4948		0.1716
1	BCC	0.2973	0.8113	0.02629
	C14 Laves	0.4959		0.1728
5	BCC	0.2968	0.8064	0.02615
	C14 Laves	0.4925		0.1694

distinct crystallographic phases, namely, BCC phase of dendritic shape, C14 Laves phase with a network shape and the white lard phase with irregular shape which increases together with x, as confirmed by XRD. Table 2 shows that the main component of the BCC phase is composed of V, Cr and Ni, while the main component of the C14 Laves phase is composed of Ni, Zr and V. Under our experimental conditions, identification of the chemical composition and structue of the new specimen is not possible. However, from semi-quantitative EDS analysis shown in Fig. 3 and Table 2, it is certain that the new specimen is of a Zr-rich phase and its main components are Zr, V and Ni with a small quantity of other elements, including La, Al, Cr, Ti, Co, Mn, which disagrees with the reported result that La is not soluble in alloying elements of AB_2-type metal hydride except Ni [19].

3.2 Activation properties and maximum capacity

Figure 4 illustrates the discharge capacity versus cycle number of TVS + x% AB_5 ($x = 0, 1, 5$) alloy electrodes. The number of activation cycles for all composite alloy electrodes decreases remarkably with increasing AB_5 alloy addition. TVS alloy requires 19 activation cycles, however it only needs 7 and 4 activation cycles when $x = 1, 5$, respectively. Tsukahara et al. [6] pointed that the single V-based solid solution phase has no electrochemical discharge capacity in KOH electrolyte because it is not an electro-catalyst. But with the presence of other phases in the V-based alloys such as TiNi phase or C14 Laves, which

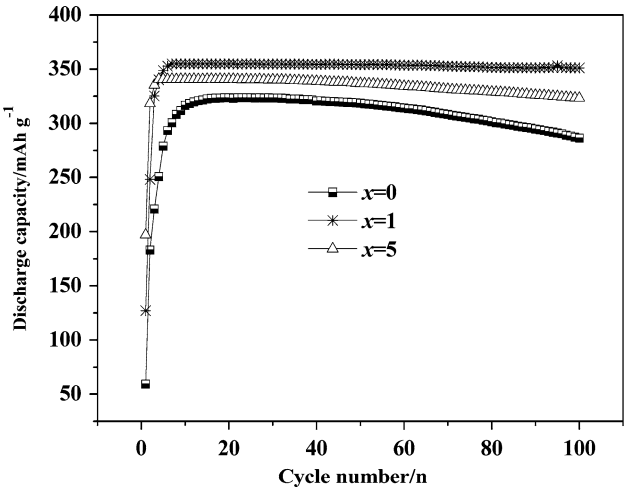

Fig. 4 Charge–discharge cycle curve of TVS + x% AB_5 ($x = 0, 1, 5$) alloy electrode

acts as a catalyst or a micro-current collector, the V-based solid solution phase will be activated to absorb and desorb reversibly a considerable amount of hydrogen in KOH electrolyte. As mentioned above, the amount of the new specimen in the composite alloys increases with x, and furthermore, it may form active sites and pathways for hydrogen diffusion [6, 13, 19]. In addition, the phase boundaries increase with the number of phases, and diffusion through grain boundaries with open structure is easier than that in grains with a perfect lattice structure [20]. As a result, the activation of the composite alloys is improved dramatically as x increases. Therefore, it is suggested that C14 Laves phase, and especially BCC phase, are the hydrogen storage phases in the composite alloys, and C14 Laves phase and the new specimen may work mainly as a catalyst or a micro-current collector.

Meanwhile, the maximum discharge capacity of the alloy electrode shown in Fig. 4 first increases from 323.6 mAh g^{-1} ($x = 0$) to 354.9 mAh g^{-1} ($x = 1$) and then decreases to 340.8 mAh g^{-1}($x = 5$) with increasing x, and composite TVS + 1% AB_5 alloy electrode has higher discharge capacity. This may be ascribed to changes in cell volume of the BCC phase which is the major storage hydrogen phase, the larger interstitial position of the BCC phase in the lattice and the greater benefit to the hydrogen storage process. As mentioned above, the cell volume of

Table 2 Phase composition for TVS + 5% AB_5 composite alloy

Phase	Composition (atom%)								
	Ti	Zr	V	Cr	Ni	Al	Mn	Co	La
BCC	0.34	3.53	68.94	12.54	11.00	0.54	2.11	0.99	–
C14 Laves	9.93	23.53	20.78	6.13	29.03	6.31	2.12	2.18	–
New specimen	5.22	33.10	24.85	6.55	12.07	7.27	1.23	1.80	7.92

the BCC phase first increases and then decreases with increasing x, and it is the largest when $x = 1$, as shown in Table 1.

3.3 Cyclic durability

The cyclic durability of the TVS + x% AB_5 ($x = 0$, 1, 5) alloy electrode is also presented in Fig. 4. The capacity retention used to represent the cycling stability can be calculated using the following equation:

$$S_n(\%) = C_n \times 100/C_{\max} \quad (1)$$

where S_n and C_n are the capacity retention and the discharge capacity at cycle number n, respectively. $C_{\max}$ is the maximum discharge capacity. It can be calculated that the capacity retention of TVS + x% AB_5 ($x = 0$, 1, 5) alloy electrode after 100 cycles is 88.50%, 98.93%, and 94.89%, respectively. This suggests that the cyclic durability of the TVS alloy electrode is also improved by adding AB_5 alloy. To elucidate the improvement, the concentrations of the constituent elements dissolved in KOH electrolyte are analyzed by ICP-OES (iCPA6000, Thermo Scientific, USA) measurement at the 50th and 100th cycles, respectively, and the results are listed in Table 3. It can be seen that the dissolution of Ti, Zr and V elements first decrease and then increase with x, which means that a small amount (1%) of AB_5 alloy is helpful in restricting the dissolution of Ti, Zr and V elements, but a mass of AB_5 alloy accelerates the dissolution of Ti, Zr and V elements. Consequently, a small amount (1%) of AB_5 alloy may improve cyclic durability of TVS alloy and a mass of AB_5 alloy addition may deteriorate the cycling stability. As is well known, V is a main hydrogen absorbing element, and the dissolution of vanadium would lead to capacity degradation of the electrode, and dissolution of Zr in C14 Laves phase would lead to a decrease in the electrocatalytic activity of the alloy [21], and segregation of Zr-rich phase may restrain the lattice expansion of metal hydride and decrease the pulverization rate [22]. This is why that the addition of AB_5 type alloy into TVS alloy adversely affects the advantageous effects of the dissolution of Ti, Zr and V elements to the cycling durability of the alloy.

3.4 Temperature effect

In order to examine the effect of temperature on the composite alloy, the discharge ability at different temperatures is denoted as the ratio of the discharge capacity C_T at a certain temperature to the discharge capacity C_{303} at 303 K. Fig. 5 shows the discharge ability at different temperatures for the TVS + x% AB_5 ($x = 0$, 1, 5) alloy electrode. It is obvious that the discharge capacity is very sensitive to temperature within a certain temperature range. The matrix TVS alloy electrode reaches its maximum discharge capacity at 303 K: the discharge capacity then declines with decreasing temperature, and it is not sensitive to temperature within the temperature range 303 K–343 K. However, the composite alloy electrode is quite different. Its discharge capacity reaches its maximum at 293 K, and then gradually decreases below or above 293 K. It can be easily found that adding AB_5 alloy can be helpful in increasing the low temperature discharge ability (LTD) of the composite alloy electrode. For example, the LTD is 12.25% when $x = 0$ but 60.26% when $x = 5$ at 233 K. Because the discharge process of the alloy electrode at low temperature is controlled by hydrogen diffusion, and the more grain boundaries an open structure has, the easier can

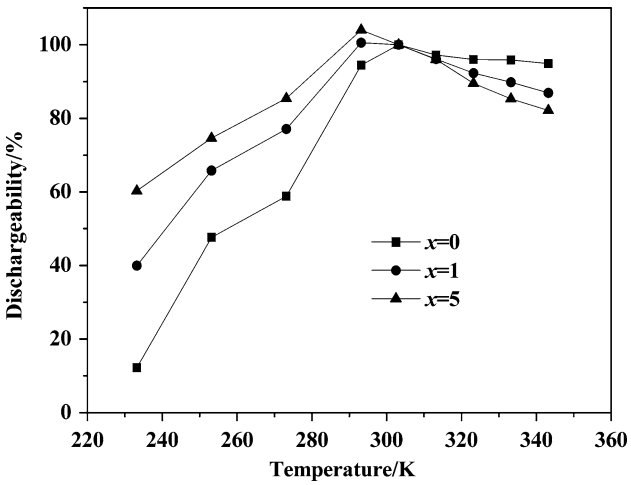

Fig. 5 Dependence of dischargeability on temperature for TVS + x% AB_5 ($x = 0$, 1, 5) alloy electrode

Table 3 Electrochemical kinetic parameters and dissolution of constituent elements in KOH electrolyte at different cycles for TVS + x% AB_5 ($x = 0$, 1, 5) alloy electrode

Sample	Charge transfer resistance, R_{ct} (mΩ)	Exchange current density, I_0 (mA g^{-1})	Hydrogen diffusion coefficient, D (10^{-10} cm^2 s^{-1})	Concentration in KOH (mg L^{-1})					
				50 cycles			100 cycles		
				Ti	Zr	V	Ti	Zr	V
$x = 0$	112.3	232.61	12.28	0.034	13.57	31.11	0.088	27.43	74.14
$x = 1$	83.74	311.94	18.29	0.018	12.65	26.10	0.081	18.14	52.14
$x = 5$	71.74	364.12	20.39	0.026	13.07	28.62	0.106	22.34	61.85

hydrogen be diffused in the alloy bulk, the increased number of grain boundaries with increasing x doubtlessly lead to its superior LTD for composite alloy. However, the high temperature discharge ability (HTD) of the composite alloy electrode is lower than that of matrix the TVS alloy. Unfortunately, we cannot fully explain this phenomenon and perhaps significant self-discharge at higher temperature is a dominant reason.

3.5 High-rate dischargeability and electrochemical kinetics

Figure 6 shows the high-rate dischargeability (HRD) for TVS + x% AB_5 (x = 0, 1, 5) alloy electrode. The HRD is calculated using the following equation:

$$\mathrm{HRD}(\%) = C_i \times 100/C_{60} \quad (2)$$

where C_i refers to the discharge capacity at different discharge rates (keeping the charge current density as 60 mA g^{-1}), C_{60} refers to the discharge capacity at both the charge/discharge current density of 60 mA g^{-1}. It shows that the HRD of alloy electrode is notably improved when AB_5 alloy is added. For example, at a discharge current density of 1,500 mA g^{-1}, the HRD increases from 30.19% (x = 0) to 63.06% (x = 5). According to electrochemical theory, the discharge process of hydrogen storage alloy includes five consecutive steps: (1) the hydride (β) is transformed into the solid solution (α) phase; (2) absorbed hydrogen diffuses from the interior to the surface of the alloy particles; (3) absorbed hydrogen is transformed into adsorbed hydrogen on the surface of the alloy particles; (4) hydrogen is transferred from adsorbed state to desorbed state; (5) desorbed hydrogen engages in charge transfer reactions on the surface of the alloy particles. Generally speaking, the HRD of the alloy electrode is believed to be mainly controlled by both the charge-transfer resistance at the electrode/electrolyte interface and hydrogen diffusion in the bulk alloy [23]. In order to investigate the kinetics of the alloy electrode, electrochemical impedance spectroscopy (EIS) and potentiostatic discharge were employed.

Figure 7 presents the EIS for TVS + x% AB_5 (x = 0, 1, 5) alloy electrode at 50% DOD. The EIS spectrum consists of two semicircles at high frequency and a short straight line at low frequency, and the radius of the larger semicircle in the high frequency region decreases with increasing x. According to the model proposed by Kuriyama et al. [24], the smaller semicircle in the high frequency region is mainly related to the contact resistance and capacitance between the alloy particles and conductive material, while the larger semicircle in the high frequency region is attributed to the charge transfer resistance for the dehydrogenation reaction on the alloy surface. The charge-transfer resistance R_{ct} is calculated by area-normalized EIS analysis, and the exchange current density I_0 is obtained by the following equation as the over-potential is very small:

$$I_0 = (RT/F)(1/R_{ct}) \quad (3)$$

where R is the gas constant, T is the absolute temperature and F is the Faraday constant. R_{ct} and I_0 are tabulated in Table 3. R_{ct} at the surface of the alloy electrode decreases from 112.3 mΩ (x = 0) to 71.74 mΩ (x = 5) and accordingly I_0 increases from 232.61 mA g^{-1}(x = 0) to 364.12 mA g^{-1} (x = 5) with increasing x, which inevitably leads to an increase in HRD when AB_5 alloy is added, as is shown in Fig. 6. Generally speaking, I_0 is commonly used to characterize the electrocatalytic activity for charge transfer reactions at the electrode/electrolyte interface. As mentioned above, the amount of the new specimen increases with increasing AB_5 alloy content. Therefore, it

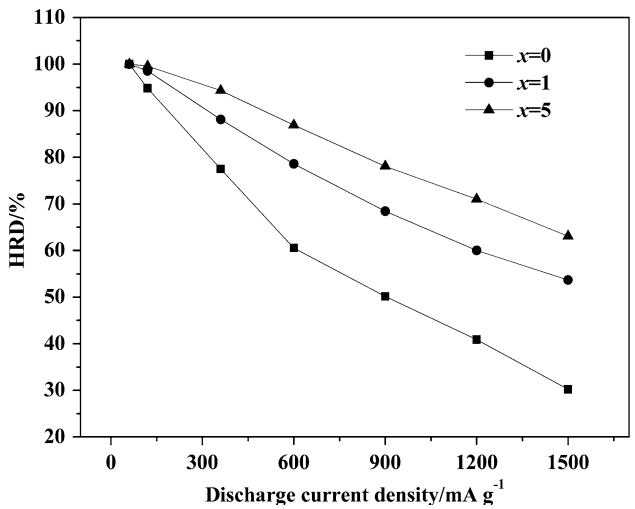

Fig. 6 HRD of TVS + x% AB_5 (x = 0, 1, 5) alloy electrode

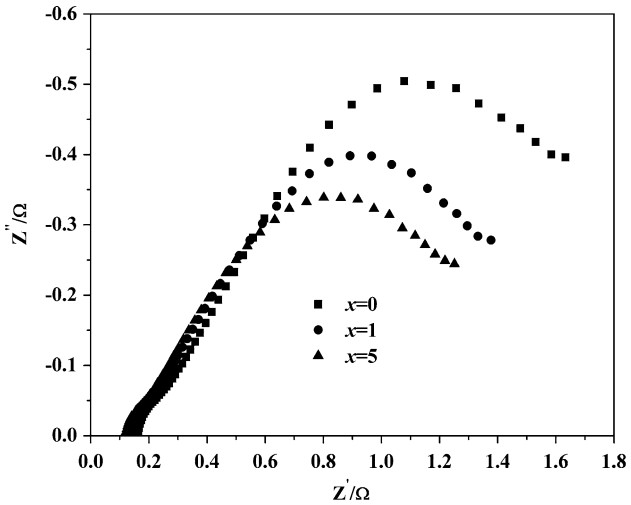

Fig. 7 Electrochemical impedance spectrum of TVS + x% AB_5 (x = 0, 1, 5) alloy electrode

is suggested that the new specimen containing La is a good electrocatalyst for charge-transfer reactions on the alloy electrode. This hypothesis needs further verification.

The hydrogen diffusion coefficient is used to characterize the hydrogen diffusion rate in the alloy. It is determined by the potential-step method for TVS + x% AB_5 (x = 0, 1, 5) alloy electrode. According to the model of Zheng et al. [25], the hydrogen diffusion coefficient in the alloy bulk is estimated and also tabulated in Table 3. The hydrogen diffusion coefficient increases from 12.28×10^{-10} cm^2 s^{-1}($x = 0$) to 20.39×10^{-10} cm^2 s^{-1} ($x = 5$) with increasing x. this may be ascribed to the following: abundant defects and grain boundaries in the multiphase composite alloy provide good channels for hydrogen diffusion and hydrogen diffusion avoids long-range diffusion through an already formed hydride.

According to Iwakura et al. [26], if the electrochemical kinetics at the electrode/electrolyte interface is the rate-determining factor, a linear dependence of HRD on the exchange current density should be observed. Similarly, if the hydrogen diffusion in the bulk alloy is the rate-determining factor, a linear dependence of HRD on hydrogen diffusion coefficient should be observed. Figure 8 shows HRD as a function of exchange current density and hydrogen diffusion coefficient for melted TVS + x% AB_5 ($x = 0, 1, 5$) alloy electrode at a discharge current density of 1,500 mA g^{-1}. The HRD shows a linear relationship with I_0 and D respectively, which implies that in the present study, both the charge-transfer reaction of hydrogen at the electrode/electrolyte interface and hydrogen diffusion in the alloy bulk are responsible for the improvement in the HRD at a discharge current density of 1,500 mA g^{-1}.

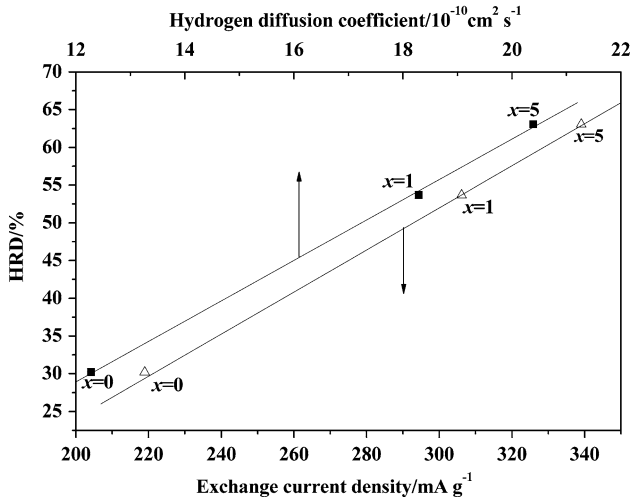

Fig. 8 HRD at 1500 mA g^{-1} as a function of exchange current density and hydrogen diffusion coefficient for TVS + x% AB_5 ($x = 0, 1, 5$) alloy electrode

4 Conclusions

The effects of AB_5 alloy on the structure and electrochemical characteristics of TVS hydrogen storage alloys have been investigated and the main conclusions are:

(1) The main phase of the composite alloys remains unchanged when AB_5 alloy is added. However, a new specimen is formed, and the amount of the new specimen increases with increasing AB_5 content. The lattice parameters and cell volumes of the BCC phase and C14 Laves phase increase as x increases from 0 to 1 and decrease as x increases further. V-based solid solution phase is mainly composed of V, Cr and Ni. C14 Laves phase is mainly composed of Ni Zr, and V, and the new specimen containing La in Zr-rich phase is mainly composed of Zr, V and Ni.

(2) The electrochemical characteristics of the composite alloys are dramatically improved with increasing AB_5 alloy content. The charge-transfer resistance R_{ct} at the surface of the alloy electrode decreases from 112.3 mΩ ($x = 0$) to 71.74 mΩ ($x = 5$) and accordingly I_0 increases from 232.61 mA g^{-1}($x = 0$) to 364.12 mA g^{-1}($x = 5$) with increasing x. The hydrogen diffusion coefficient increases from 12.28×10^{-10} cm^2 s^{-1}($x = 0$) to 20.39×10^{-10} cm^2 s^{-1}($x = 5$) with increasing x. The activation cycle number decreases from 19 cycles ($x = 0$) to 4 cycles ($x = 5$). The HRD increases from 30.19% ($x = 0$) to 63.06% ($x = 5$) at a discharge current density of 1,500 mA g^{-1}. The LTD increases from 12.25% (x = 0) to 60.26% ($x = 5$) at 233 K. The maximum discharge capacity increases from 323.6 mAh g^{-1} ($x = 0$) to 354.9 mAh g^{-1}($x = 1$), then decreases to 340.8 mAh g^{-1}. The capacity retention after 100 cycles first increases from 88.50% ($x = 0$) to 98.93% ($x = 1$) and then decreases to 94.89% ($x = 5$).

(3) The HRD is controlled by the charge-transfer reaction of hydrogen and the hydrogen diffusion in the bulk of the alloy under the present experimental conditions.

Acknowledgments This work was supported by Foundation of State Key Laboratory of Rare Earth Resource Utilization, Changchun Institute of Applied Chemistry, Chinese Academy of Sciences. We thank Dr. Taicheng Duan of Key Laboratory of Rare Earth Resource Utilization, Changchun Institute of Applied Chemistry, Chinese Academy of Sciences for ICP test, and Ms. Yan Wang and Dr. Wentao Hu of State Key Laboratory of Metastable Materials Science and Technology, Yanshan University for SEM and XRD measurements.

References

1. Feng F, Geng M, Northwood DO (2001) Int J Hydr Energy 26:725
2. Guo R, Chen LX, Lei YQ et al (2003) Int J Hydr Energy 28:803
3. Kohno T, Yoshida H, Kanda M (2004) J Alloys Compd 363:249
4. Tsukahara M, Takahashi K, Mishima T et al (1995) J Alloys Compd 226(1):203

5. Tsukahara M, Takahashi K, Mishima T et al (1995) J Alloys Compd 224:162
6. Tsukahara M, Takahashi K, Mishima T et al (1997) J Alloys Compd 253:583
7. Kuriyama N, Tsukahara M, Takahashi K et al (2003) J Alloys Compd 356:738
8. Kim JH, Lee H, Lee PS et al (2003) J Alloys Compd 348:293
9. Zhang QA, Lei YQ, Yang XG et al (2000) J Alloys Compd 305:125
10. Yan YG, Chen YG, Liang H et al (2006) J Alloys Compd 426:253
11. Chai YJ, Zhao MS (2005) Int J Hydr Energy 30:279
12. Chai YJ, Yin WY, Li ZY et al (2005) Intermetallics 13:1141
13. Qiao YQ, Zhao MS, Zhu XJ et al (2007) Int J Hydr Energy 32:3427
14. Dos Santos DS, Bououdina M, DInt Fruchart (2003) J Hydr Energy 28:1237
15. Chu HL, Zhang Y, Sun LX et al (2007) J Alloys Compd 614:446
16. Yu XB, Li F, Wu Z et al (2004) Physics Letters A 320:312
17. Bououdina M, Sun DL, Enoki H (1999) J Alloys Compd 288:229
18. Han SM, Zhang Z, Zhao MS et al (2006) Int J hydr Energy 31:563
19. Seo CY, Choi SJ, Choi J et al (2003) J Alloys Compd 351:255
20. Park HY, Chang I, Cho WI et al (2001) Int J Hydr Energy 26:949
21. Qiao YQ, Zhao MS, Li MY et al (2006) Scripta Materialia 55:279
22. Seo CY, Choi SJ, Choi J et al (2003) Int J Hydr Energy 28:317
23. Liu YF, Pan HG, Gao MX et al (2004) J Alloys Compd 365(1):246
24. Kuriyama N, Sakai T, Miyamura H et al (1993) J Alloy Compd 202:183
25. Zheng G, Popov BN, White RE et al (1995) J Electrochem Soc 142:2695
26. Iwakura C, Oura T, Inoue H et al (1996) Electrochim Acta 41(1):117